Improvements in a 20-kW Phase-Locked Magnetron by Anode Voltage Ripple Suppression

Xiaojie Chen, Ze Yu, Hang Lin, Xiang Zhao, and Changjun Liu, *Senior Member, IEEE*

***Abstract*— Microwave devices based on high-power magnetrons are currently used widely and there is a strong demand for phase-controlled magnetrons. In this work, the performance of a 20-kW *S*-band continuous-wave magnetron with varied anode voltage ripple is studied. The anode voltage ripple is introduced to an equivalent model of the magnetron to evaluate the system's performance theoretically. The effects of the anode voltage ripple and the injection parameters on the magnetron's output are thus analyzed numerically. Furthermore, experiments are performed while the anode voltage ripple is varied from 4.2% to 0.6% using a shunt capacitance-adjustable ripple filter module. A nearly tripled locking bandwidth is observed under a constant injection ratio at 0.1 with decreasing ripple. The ripple-suppressed system pulls its sideband energy to the locking frequency and thus achieves a spectral intensity increment of 0.9 dB, phase noise reduction of 13 dB at an offset of 100 kHz, and phase jitter convergence from ±1.8° to ±0.9°. The experimental features validate the results obtained from the theoretical analyses. The results of this investigation also provide guidance for future industrial applications of phase-locked magnetron arrays.**

***Index Terms*— Anode voltage ripple, locking bandwidth, phase-locked magnetron, spurious suppression.**

I. Introduction

SPACE solar power stations (SSPSs) [1], microwave material processing, particularly in the microwave chemical vapor deposition field [2], microwave sintering of powdered metals [3], and other technological innovations rely on promising high-power microwave technologies that enable energy savings and emission reduction. High-power microwave sources are also indispensable in high-energy physics, e.g., for driving the superconducting radio frequency cavities of a particle accelerator [4]. The magnetron is a widely used type of power device that offers high power capacity, high efficiency, and low cost. Self-oscillated magnetrons cannot be applied directly in phase-controlled applications because of their random phase fluctuations and wide spectral bands [5]. Furthermore, various electrical devices are vulnerable within the frequency range of the extensively applied *S*-band magnetrons; for example, Zigbee sensors, Bluetooth equipment, Wi-Fi communication devices, and other systems that conform to the IEEE 802.11 b/g/n are at high risk of electromagnetic interference from magnetrons.

Therefore, overcoming the problems of the noisy microwave output of a magnetron has attracted significant research attention when the device is selected for use as a microwave source. Mitani *et al.* [6] proposed turning off the filament current of a magnetron as a valid method to improve an oven magnetron's output when the filament works well with reshock electrons. However, magnetrons are usually difficult to operate for long periods in the cathode-off method. Mitani *et al.* [7] further proposed a cathode shield technique that greatly suppressed spurious noise by preventing the electrons from the cathode end-portion from going into the anode–cathode (A-K) gap. Neculaes *et al.* [8] concentrated on field effects in the electronic interaction space in ovens and in relativistic magnetrons, in which the noises near the carrier frequency are suppressed significantly by axially asymmetric azimuthal variation of the axial magnetic field. Another widely applied method involves the application of external injection locking to a magnetron to solve the unstable output in terms of both phase and frequency. In recent years, the applications of phase-locking magnetrons have entered a period of diversification. Shinohara [9] successfully proposed the power-variable phase-controlled magnetron technique, which is intended to be applied to an SSPS source array, using injection locking and phase-locked loop feedback to the anode current. Dexter *et al.* [10] first demonstrated that the single-cell superconducting cavity of a particle accelerator could be driven precisely using a phase-locked magnetron. Modulated signals were achieved by injection locking of magnetrons for communications applications by Tahir *et al.* [11] and Yang *et al*. [12]. Liu *et al.* [13], Huang *et al.* [14], and Liu *et al.* [15] concentrated on high-efficiency coherent power combining based on a multipath phase-locked magnetron to satisfy the increasing demand for power from the microwave industry. Therefore, it is important to improve the output spectra of phase-locked magnetrons to achieve a wider locking bandwidth and a stable phase output. Such magnetrons are expected to satisfy more applications and reduce any electromagnetic interference in the adjacent channels.

The effects of anode voltage ripple on a phase-locked magnetron are rarely reported. This article presents an approach to improve this type of magnetron's output performance by

Manuscript received August 29, 2019; revised October 26, 2019; accepted November 17, 2019. Date of publication December 31, 2019; date of current version June 10, 2020. This work was supported in part by the NSFC under Grant 61931009 and in part by the National Basic Research Program of China (973 Program) under Grant 2013CB328902. The review of this article was arranged by Senior Editor D. A. Shiffler, Jr. *(Corresponding author: Changjun Liu.)*

The authors are with the School of Electronics and Information Engineering, Sichuan University, Chengdu 610064, China (e-mail: cjliu@ieee.org).

Color versions of one or more of the figures in this article are available online at http://ieeexplore.ieee.org.

Digital Object Identifier 10.1109/TPS.2019.2956868

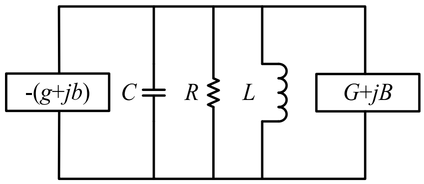

Fig. 1. Equivalent circuit of a magnetron with a load.

smoothing its anode voltage. In Section II, various anode voltage ripples are introduced into a theoretical magnetron model and their effects on the locking performance are analyzed numerically. A phase-locked 20-kW S-band continuous-wave (CW) magnetron system with suppressed anode voltage ripples is presented. The experimental setup is described in Section III. In Section IV, the locking bandwidth, the spectral purity, and the phase stability of the magnetron are investigated experimentally and discussed. This is the first time that the correlation between the output of a high-power magnetron and the anode voltage ripples has been demonstrated.

II. Theory and Analysis

A. Theoretical Analysis of Phase-Locked Magnetron

The phase-locking principle and the physical mechanism of a magnetron have still not been fully explained theoretically. According to Slater's theory, a single-mode operating (usually π mode) magnetron can be equivalent to a parallel resonant circuit composed of lumped components [16], as shown in Fig. 1. The electron admittance is represented by $-(g+jb)$; the magnetron resonance cavity is approximated by a resistor–inductor–capacitor (RLC) resonant circuit; and the external load is then regarded as the load admittance $G+jB$. We then obtain

$$\frac{g+jb}{C\omega_0} = j\left(\frac{\omega}{\omega_0} - \frac{\omega_0}{\omega}\right) + \frac{1}{Q_0} + \frac{G+jB}{Q_{\rm ext}} \tag{1}$$

where ω is the magnetron's output frequency, ω_0 is the resonance frequency of the resonant cavity, and $Q_0 = RC\omega_0$ and $Q_{\rm ext}$ are the unloaded and external loaded quality factors, respectively. Q_0 and $Q_{\rm ext}$ show the coupling between the load and the magnetron.

An external signal at a frequency around ω_0 is injected into a magnetron to act as a reference. The power of this signal is much lower than the output power of the magnetron. According to Chen's investigations, the instantaneous microwave output amplitude $V_{\rm MW}$, the angular frequency $\omega_{\rm MW}$, and the phase change rate $d\varphi/dt$ between the reference signal and the magnetron can be derived individually as follows [17]:

$$V_{\rm MW} = V_{\rm MW0}\frac{1}{1+\frac{\rho\omega_0\cos\varphi}{2\gamma Q_{\rm ext}}} \tag{2}$$

$$\omega_{\rm MW} = \omega' + \frac{\omega_0\rho}{2Q_{\rm L}}(\sin\varphi - \cos\varphi\cdot\tan\alpha) \tag{3}$$

$$\frac{d\varphi}{dt} = \omega_0\frac{\rho}{2Q_{\rm ext}}\sin\varphi + \omega_{\rm MW} - \omega_1 \tag{4}$$

where γ is defined as a growth parameter, α is a constant called the pushing parameter, $V_{\rm dc}$ is the DC voltage across the A-K gap, ω_1 is the angular frequency of the injected signal, $\rho = (P_{\rm in}/P_0)^{1/2}$ is the injection ratio, and $Q_{\rm L}$ is the loaded quality factor. φ is the phase difference between the reference signal and the magnetron output, while $V_{\rm MW0}$ and ω' are the instantaneous microwave amplitude and the frequency of the self-oscillated magnetron, respectively. We then obtain

$$V_{\rm MW0} = \frac{V_{\rm dc}}{1+\frac{C\omega_0 R}{Q_{\rm L}}} \tag{5}$$

$$\omega' = \omega_0 + \frac{b_0}{2C} - \frac{B\omega_0}{2Q_{\rm ext}} - \frac{\omega_0\tan\alpha}{2Q_{\rm L}} \tag{6}$$

where b_0 is a constant.

Apparently, the phase-locking state can be derived analytically from (4) by setting $d\varphi/dt = 0$. Then, we obtain the classical Adler's condition, which is read as

$$\frac{\rho\omega_0}{2Q_{\rm ext}} \geq |\omega_{\rm MW} - \omega_1|. \tag{7}$$

To investigate the locking bandwidth and the amplitude of the phase-locking magnetron, we then combine (2) and (4) by canceling their φ dependence. The locking scope governing equation is given as

$$\frac{(V_{\rm REL}-1)^2}{(\mu/\gamma)^2} + \left(\frac{\sigma}{\mu}\right)^2 = 1 \tag{8}$$

where $V_{\rm REL} = V_{\rm MW}/V_{\rm MW0}$ represents the relative voltage of the locking and self-oscillated outputs, $\mu = \rho/2Q_{\rm ext}$ represents the injection amplitude, and $\sigma = (\omega_{\rm MW} - \omega_1)/\omega_0$ represents the relative locking bandwidth and suggests that all frequencies are normalized with respect to ω_0. Equation (8) shows an ellipse function when both μ and σ are real.

To investigate the performance of the phase-locked magnetron, we assume that its anode voltage consists of the constant DC voltage $V_{\rm dc}$ and the comparatively slow fluctuation $\delta V(t)$

$$V'_{dc} = V_{dc} + \delta V(t) \tag{9}$$

where δV(t) represents a small random ac component of the anode voltage that is introduced by the dc power supply. By substituting (9) into (5), we find that the DC voltage amplitude of a self-oscillated magnetron fluctuates with δV(t) as a ripple. The electronic admittance $g + jb$ changes with variation in $V_{\rm dc}$ [16], [17]. The load susceptance B is also affected by $V_{\rm dc}$ because of the balance of the imaginary part in (1). Therefore, (6) indicates that the self-oscillated frequency shifts with various rippled values of $V'_{\rm dc}$.

Because of its slowly varying characteristic and the diverse range of ripples caused by the various types of power supply, we believe that the anode voltage with fluctuating components can be regarded as a root-mean-square (rms) voltage, and (9) is then modified to read

$$V'_{\rm dc} = V_{\rm dc}\left(1+\frac{S}{2\sqrt{2}}\right) \tag{10}$$

where S is the ripple parameter determined using $S = V_{\rm p-p}/V_{\rm dc}$, where $V_{\rm p-p}$ is the peak-to-peak value of the fluctuation. Substitution of (10) into (8) gives

$$\frac{\left\{V_{\rm REL}/\left[1+S/\left(2\sqrt{2}\right)\right]-1\right\}^2}{(\mu/\gamma)^2} + \left(\frac{\sigma}{\mu}\right)^2 = 1 \tag{11}$$

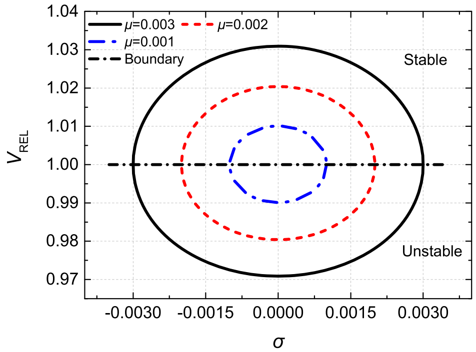

Fig. 2. Theoretical phase-locking performance of magnetron with various values of injection parameter σ.

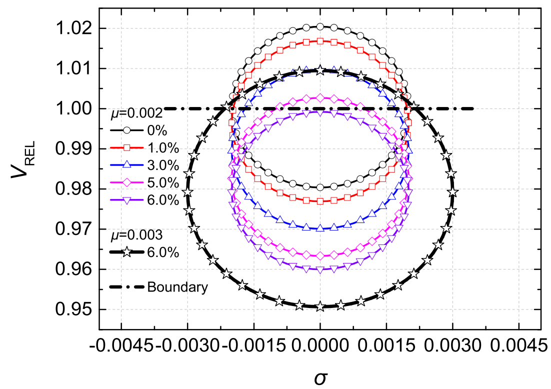

Fig. 3. Phase-locking performance of magnetron with respect to the anode voltage ripple S.

which describes both the amplitude and the bandwidth of a phase-locked magnetron with respect to its anode voltage ripple.

B. Numerical Analysis of Phase-Locked Magnetron With Anode Voltage Ripple

To aid in the theoretical analysis, ω_0 is defined to have a constant value of 1. Based on the results suggested by Woo *et al.* [18], the typical values of γ/ω_0 range between 0.1 and 0.167. Therefore, we select the value of $\gamma/\omega_0 = 0.1$ for later analysis.

The curves of V_{REL} with respect to σ are shown in Fig. 2. Each curve is plotted with respect to an injection amplitude. All ellipses of locking status have a common geometric center, e.g., $\sigma = 0$ and $V_{REL} = 1$, which represents the self-oscillation condition. Each ellipse shown in Fig. 2 can be divided into two parts. The boundary is determined by $V_{REL} = 1$, as indicated by the short-dash-dotted line in Fig. 2. If the stability condition $\cos(\varphi_{lock}) \leq 0$ is established, then the phase-locked magnetron operates at the upper branch with $V_{REL} > 1$, which is consistent with reality. Otherwise, if there is a negative solution to (8) like that on the lower branch, then the operating condition is not satisfied.

The injection amplitude μ in our simulation varies from 0.001 to 0.003 with intervals of 0.001. The locking bandwidth σ in the stable state is represented by two symmetrical points where the ellipse intersects with the boundary line $V_{REL} = 1$. Fig. 2 clearly shows that the magnetron can only be phase-locked when (7) is satisfied.

When the injection amplitude increases, the locking bandwidth extends to become wider and the output power also rises. In addition, the maximum output power is obtained when the injected locking signal has a zero frequency deviation ($\sigma = 0$). When the frequency deviation is equal to or greater than μ, no locking status can be achieved.

To analyze the effects of the anode voltage ripple on the magnetron locking condition, we set several reasonable ripples of around 5.0% to analyze the device performance. The effects of the ripple parameter S on the locking results are illustrated in Fig. 3, where the anode voltage ripple parameter S has values of 1.0%, 3.0%, 5.0%, and 6.0%, while the injection amplitude remains at $\mu = 0.002$. The stable branches shown in Fig. 3 are used to evaluate the magnetron's locking performance with respect to the anode voltage ripple. The anode voltage with zero ripple will lead to the maximum locking bandwidth, which is the prediction of Adler's equation as well. When the ripple varies from 0% to 5.0%, the stable branch moves downward. The magnetron's output voltage at the locking condition has also decreased because of the ripples. When the anode voltage ripple reaches 5.0%, the phase-locking condition may be achieved using only a small-σ injection near the central frequency of the magnetron in self-oscillation mode. However, when the ripple reaches 6.0%, the state ellipse has no intersections with the boundary line where $V_{REL} = 1$. This implies that the magnetron is operating in the unstable region and no phase-locking may be achieved.

TABLE I
THEORETICAL PHASE-LOCKING RESULTS WITH INCREASING ANODE VOLTAGE RIPPLE

Ripple parameter	Amplitude	Locking bandwidth
0%	1.0204	0.00200
1.0%	1.0168	0.00190
3.0%	1.0097	0.00170
5.0%	1.0027	0.00091
6.0%	0.9992	N/A

The amplitude is the phase-locked output voltage versus the self-oscillated output voltage V_{REL}, and the locking bandwidth is the normalized frequency difference given by $(\omega_1 - \omega_{MW})/\omega_0$.

The results for the amplitude and the locking bandwidth are presented in Table I. In addition, the performance deterioration caused by the anode voltage ripples can be significantly overcome by increasing the injection amplitude μ to 0.003, as also shown in Fig. 3. However, this may cause the cost of the injection subsystem to rise greatly and is not recommended for applications in industrial applications.

III. EXPERIMENTAL SETUP

To explore the effects of the anode voltage ripples on the phase-locked magnetron's performance and verify our theoretical analysis, we have also developed a corresponding

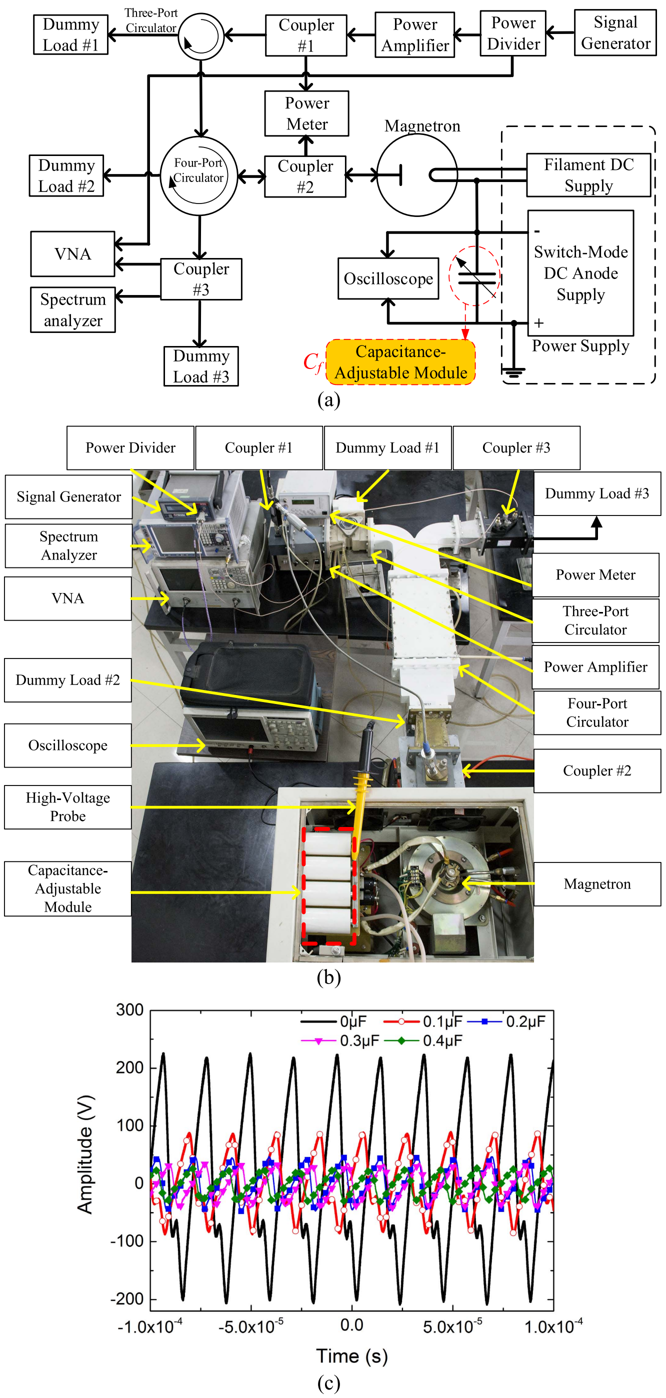

Fig. 4. Phase-locked magnetron system with variable anode voltage ripple and its behavior. (a) Diagram of phase-locked magnetron system. (b) Photograph of the experimental system. (c) Measured ripple waveforms with respect to various filtering capacitances.

experimental system. The system diagram is shown in Fig. 4. The magnetron was manufactured by Sanle Microwave Co., Nanjing, China, (model: CK-2091) with a maximum output power of 20-kW CW at 2.45 GHz.

The magnetron is driven using a dc power supply (Bolei Electric Co.) that is integrated with an electromagnet supply and an anode current supply and provides a magnetic field intensity of 1250 Gs and a dc anode voltage of 10.4 kV. The dc filament current varies from 47 to 25 A as the magnetron output power is varied. A relatively sharp self-oscillated spectrum is thus achieved.

The voltage ripple of the anode voltage supply exists objectively because of nonideal rectification and filtering. We intend to control the ripple of the high-voltage supply actively to mimic various high voltage supplies with different ripple levels. Therefore, an adjustable capacitance module that is composed of four thin-film capacitors (SDD 20000 V, 0.10 μF, Eaco) is arranged in parallel to filter the ripples. Furthermore, the capacitance C_f can be tuned from 0 to 0.4 μF at intervals of 0.1 μF. An oscilloscope (DPO-7254, Tektronix) is used to measure the anode voltage ripple via a high-voltage probe (HVP-15HF, 30 dBc, Pinteck).

A reference signal is generated by a signal generator (HMC-T2220, Hittite) and amplified using a power amplifier (YYPA4D, Sanle Microwave Co.). The circulators provide a transmission path for injection of the amplified reference signal and thus protect the solid-state amplifier. The couplers are used to sample the signals to measure the power using power meters (AV2433, the 41st Institute of CETC) and the spectrum with a signal analyzer (FSV40, Rohde & Schwarz). At the same time, the time-varied phases are measured using a vector network analyzer (N5230A, Agilent). The output microwave power is absorbed by a 30-kW water-cooled dummy load.

IV. Results and Discussion

A. Self-Oscillation Spectra Versus Anode Voltage Ripples

The ripples of the anode power supply are measured when a load, i.e., the magnetron, is producing reasonable output power. The effects of the anode voltage ripples on the magnetron's performance are then investigated. The operating anode voltage and current are maintained at 10.4 kV and 2.21 A, respectively. Fig. 4(c) shows the comparison of the anode voltage ripple variations of the magnetron with various values of capacitance C_f. The ac component of anode voltage is operating at $\sim$ 50 kHz, which is the same as the operating frequency of the switch supply. It is clear that the ripple is reduced by improved filtering. While C_f increases, the ripple gradually decreases. The peak-to-peak value of the ripple decreases from 434.4 to 61.4 V, which also represents a drop in the ripple from 4.2% to 0.6%. Furthermore, the ripple suppression effect is inconspicuous when C_f is higher than 0.2 μF. Therefore, we select four ripples with values of 4.2%, 1.7%, 0.9%, and 0.6% for further investigation.

In the experiments, the magnetron's output power is maintained at 16.3 kW, while the operating anode current is tuned to 2.21 A. The central output frequency is approximately 2.4476 GHz. Fig. 5 shows the comparison of the max-hold spectra of the self-oscillating magnetron with various anode voltage ripples.

The 3-dB spectral width of the magnetron in the self-oscillating mode is improved from 2.70 to 0.93 MHz, while the anode voltage ripple varies from 4.2% to 0.6%. In addition, the spectrum amplitude stability is improved from $\pm$1.5 to $\pm$0.3 dB. These results verify the results of the theoretical analysis of the self-oscillating magnetron, which indicated that

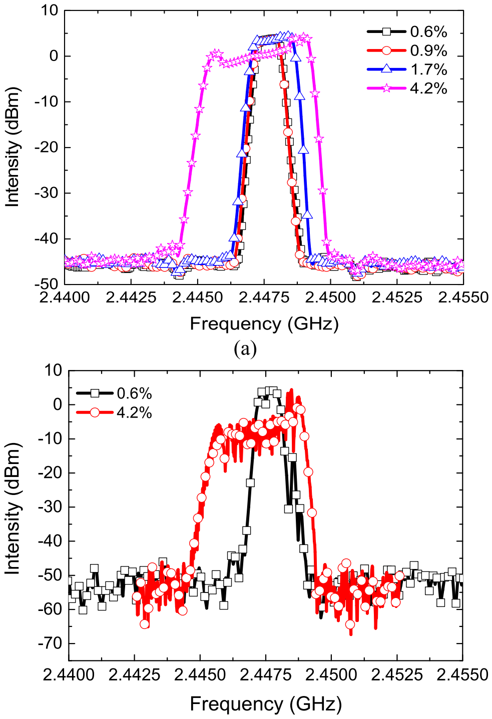

(b)

Fig. 5. Experimental spectra of the self-oscillated magnetron with respect to various anode voltage ripples [both the resolution bandwidth (RBW) and the video bandwidth (VBW) are 30 kHz]. (a) Max-hold spectra with respect to the various anode voltage ripples. (b) Free-run spectra with the worst and optimal anode voltage ripples.

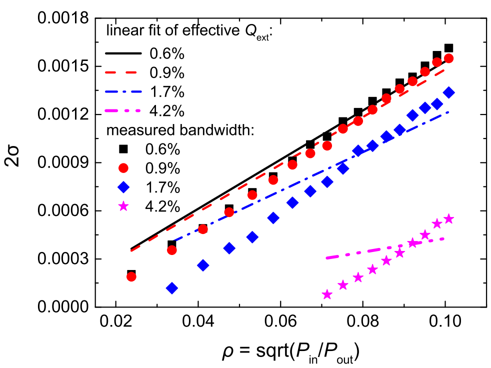

Fig. 6. Measured locking bandwidths and fitting of effective Q_{ext} factors of the magnetron for various anode voltage ripples.

as the anode voltage ripples decreased, the frequency and amplitude fluctuations also decreased in tandem.

Fig. 5(b) shows a free-run view of the magnetron spectrum with anode voltage ripples of 4.2% and 0.6%. It should be noted here that the microphonic noise still appears and is mainly caused by the magnetron's intrinsic characteristics and other active jamming phenomena.

B. Locking Bandwidth Versus Anode Voltage Ripples

The conclusions drawn earlier are illustrated for the magnetron in self-oscillation mode with anode voltage ripples $S = 4.2\%$, 1.7%, 0.9%, and 0.6%, respectively. Then, the phase-locked bandwidths are also measured. As shown in

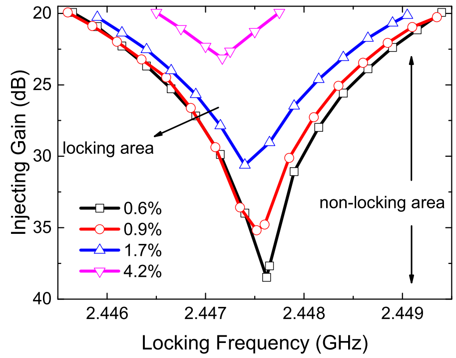

Fig. 7. Phase-locking areas with respect to the anode voltage ripples.

Fig. 6, the normalized locking bandwidth characteristics with various anode voltage ripples and injection ratios are evaluated and presented. The injection power P_{in} is tuned from 10.0 W ($\rho = 0.025$) to 180.0 W ($\rho = 0.105$) at intervals of 10.0 W. When the anode voltage ripple effects are considered, the phase locking only occurs at low injection power (< 30.0 W) when the initial anode voltage ripple is less than 2.0%. By contrast, with a high injection power at 180.0 W, the magnetron driven using the optimal voltage presents a nearly tripled locking bandwidth (3.95 MHz) when compared with the original phase-locked bandwidth (1.34 MHz).

From another perspective, the measured locking bandwidths indicate a relationship between the anode voltage ripple and the effective external loaded quality factor $Q^{\text{e}}_{\text{ext}}$ because the locking bandwidth is related to the external loaded quality factor based on Alder's equation. A lower external loaded quality factor usually leads to a broader locking bandwidth, which represents the coupling between the magnetron and the external load. The effective Q_{ext} values of the magnetron with respect to the various anode voltage ripples used in the experiments are linearly fitted to (7). As shown in Fig. 6, the slopes of these linear fitting lines are the reciprocals of the effective Q_{ext} factors. With anode voltage ripple tuning from 4.2% to 0.6%, the effective Q_{ext} factor drops from 230 to 65.

The results for the injection ratio at various injection frequencies are compiled, as shown in Fig. 7. These V-shaped curves represent the maximum injection gain with respect to the various anode voltage ripples. The region above the V-shaped curve shown in Fig. 7 represents the cases where the phase-locked states have been identified. The remaining area represents the cases where phase locking has not occurred.

The magnetron may be locked at an input power to output power ratio of 38.5 dB because of the reduction in the anode voltage ripple, while the original injection ratio was only 23.1 dB. In addition, the optimal injection-ratio frequency, i.e., the central frequency of the self-oscillating magnetron, migrated from 2.4472 to 2.4476 GHz as a result of the anode voltage ripple suppression. This phenomenon is also known as the pushing effect, where the rms value of the anode voltage is reduced by the ripples, as derived from (10).

C. Noise Performance

When Adler's condition is satisfied well with respect to the phase-locked magnetron, the spectral density of the phase

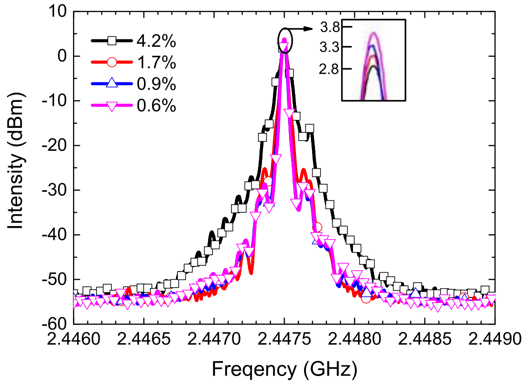

Fig. 8. Max-hold spectra of the phase-locking magnetron with respect to the various anode voltage ripples. (Both RBW and VBW are 30 kHz.)

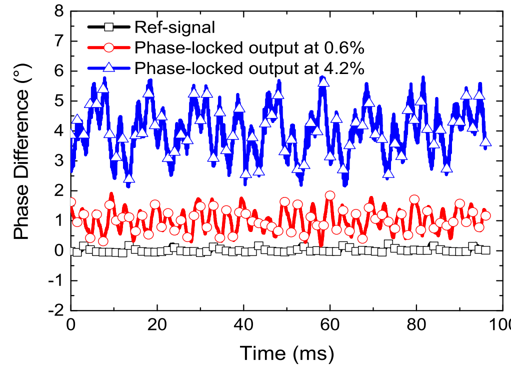

Fig. 9. Phase jitters of phase-locking with respect to various anode voltage ripples.

TABLE II

MEASURED PHASE NOISE AND PEAK OF THE SPECTRAL IDENTITY WITH RESPECT TO VARIOUS ANODE VOLTAGE RIPPLES

Ripple	Peak (dBm)	Phase noise @50 kHz	Phase noise @100 kHz
4.2%	2.89	−50.66 dBc/Hz	−57.27 dBc/Hz
1.7%	3.17	−59.89 dBc/Hz	−70.88 dBc/Hz
0.9%	3.44	−64.83 dBc/Hz	−76.10 dBc/Hz
0.6%	3.79	−66.39 dBc/Hz	−80.64 dBc/Hz

The measurements were conducted at the same injection ratio of − 22.5 dB at 2.4475 GHz.

noise can be illustrated as follows [19]:

$$|\delta\theta(\omega)|^2 = \frac{|\delta\omega(\omega)|^2}{\omega^2 + \left(\frac{\rho}{2Q_{\text{ext}}}\right)^2 - \left(\frac{\omega_1-\omega'}{\omega_0}\right)^2} \tag{12}$$

where $\delta\theta(\omega)$ is the spectral density of the phase noise and $\delta\omega(\omega)$ is the fluctuation at the self-oscillation frequency.

Obviously, because of the reduced anode voltage ripple, which provides smaller fluctuations at the self-oscillation frequency and a lower effective Q_{ext} factor, the output spectrum bandwidth of the phase-locked magnetron can be narrowed. The phase noise was improved by more than 15.0 dB at a 50-kHz offset and by over 13.0 dB at an offset of 100 kHz, as shown in Table II. Fig. 8 illustrates that the spurious power of the phase-locked magnetron is recycled into the locking frequency at 2.4475 GHz. The peak of the spectral intensity has also risen by approximately 0.9 dB, which also agrees well with the theoretical predictions. It was observed here that the 3-dB width of the phase-locked magnetron was less than 250 kHz. As the offset frequency increases further, e.g., reaching an offset of more than 1 MHz, the spectral intensities of the original state and the ripple-suppressed state are the same.

A vector network analyzer is used to monitor the phase shift between the magnetron's output and the injected microwave signal. Fig. 9 shows the measured phase jitter of the phase-locked magnetron at approximately 0.1 s. The peak-to-peak value of the injected signal was nearly constant (at less than 0.3°) and the phase fluctuation decreased from ±1.83° (original state) to ±0.9° (ripple-suppressed state), which coincided well with the results of the previous estimation.

V. CONCLUSION

In this article, the effects of anode voltage ripple on a phase-locked magnetron have been analyzed theoretically and verified experimentally in an *S*-band CW magnetron system. The anode voltage ripple parameter was introduced to the equivalent circuit model to ease the evaluation of the system behavior of the phase-locking magnetron. With the use of an adjustable-capacitance filter module, the magnetron performance has been demonstrated to improve when the anode voltage ripple decreased from 4.2% to 0.6%. With this decreasing anode voltage ripple, the output spectrum of the self-oscillating and phase-locked magnetron also narrowed. This phase-locking behavior of the magnetron is easier to achieve at lower injection levels. A lower anode voltage ripple is accompanied by a wider locking bandwidth and improved noise performance. Furthermore, our investigations indicate a way to develop a high-power but low spurious noise magnetron source with low anode voltage ripple. All these features show good agreement with the theoretical predictions.

REFERENCES

[1] W. C. Brown, "Status of the microwave power transmission components for the solar power satellite," *IEEE Trans. Microw. Theory Techn.*, vol. MTT-29, no. 12, pp. 1319–1327, Dec. 1981.

[2] J. Achard *et al.*, "High quality MPACVD diamond single crystal growth: High microwave power density regime," *J. Phys. D: Appl. Phys.*, vol. 40, no. 20, pp. 6175–6188, Oct. 2007.

[3] R. Roy, D. Agrawal, J. Cheng, and S. Gedevanishvili, "Full sintering of powdered-metal bodies in a microwave field," *Nature*, vol. 399, pp. 668–670, Jun. 1999.

[4] S. An, C. Gao, Y. S. Cho, and B. H. Choi, "PEFP low-beta SRF cavity design," in *Proc. IEEE Part. Accel. Conf. (PAC)*, Albuquerque, NM, USA, Jun. 2007, pp. 2164–2166.

[5] A. S. Gilmour, *Klystrons, Traveling Wave Tubes, Magnetrons, Crossed-field Amplifiers, and Gyrotrons*. Beijing, China: National Defence Industry Press, 2011, pp. 334–378.

[6] T. Mitani *et al.*, "Experimental research on noise reduction of magnetrons for solar power station/satellite," in *Proc. Asia–pacific Radio Sci. Conf.*, Qingdao, China, Aug. 2004, pp. 603–606.

[7] T. Mitani, N. Shinohara, H. Matsumoto, M. Aiga, N. Kuwahara, and T. Ishii, "Noise-reduction effects of oven magnetron with cathode shield on high-voltage input side," *IEEE Trans. Electron Devices*, vol. 53, no. 8, pp. 1929–1936, Aug. 2006.

[8] V. B. Neculaes *et al.*, "Magnetic perturbation effects on noise and startup in DC-operating oven magnetrons," *IEEE Trans. Electron Devices*, vol. 52, no. 5, pp. 864–871, Apr. 2005.
[9] N. Shinohara, "Beam control technologies with a high-efficiency phased array for microwave power transmission in Japan," *Proc. IEEE*, vol. 101, no. 6, pp. 1448–1463, Jun. 2013.
[10] A. C. Dexter *et al.*, "First demonstration and performance of an injection locked continuous wave magnetron to phase control a superconducting cavity," *Phys. Rev. Special Topics-Accel. Beams*, vol. 14, no. 3, Mar. 2011, Art. no. 032001.
[11] I. Tahir, A. Dexter, and R. Carter, "Frequency and phase modulation performance of an injection locked CW magnetron," *IEEE Trans. Electron Devices*, vol. 53, no. 7, pp. 1721–1729, Jul. 2006.
[12] B. Yang, T. Mitani, and N. Shinohara, "Evaluation of the modulation performance of injection-locked continuous-wave magnetrons," *IEEE Trans. Electron Devices*, vol. 66, no. 1, pp. 709–715, Jan. 2019.
[13] C. Liu *et al.*, "Experimental study on microwave power combining based on injection-locked 15-kW S-band continuous-wave magnetrons," *IEEE Trans. Plasma Sci.*, vol. 44, no. 8, pp. 1291–1297, Aug. 2016.
[14] H. Huang *et al.*, "Simulation and experiments of an S-Band 20-kW power-adjustable phase-locked magnetron," *IEEE Trans. Plasma Sci.*, vol. 45, no. 5, pp. 791–797, May 2017.
[15] Z. Liu *et al.*, "Experimental studies on a four-way microwave power combining system based on hybrid injection-locked 20 kW S-band magnetrons," *IEEE Trans. Plasma Sci.*, vol. 47, no. 1, pp. 243–250, Jan. 2019.
[16] J. C. Slater, "The phasing of magnetrons," Res. Lab. Electron., MIT Press, Cambridge, MA, USA, Tech. Rep. 35, 1947.
[17] S. C. Chen, "Growth and frequency pushing effects in relativistic magnetron phase-locking," *IEEE Trans. Plasma Sci.*, vol. 18, no. 3, pp. 570–576, Jun. 1990.
[18] W. Woo *et al.*, "Phase locking of high-power microwave oscillators," *J. Appl. Phys.*, vol. 65, pp. 861–866, Sep. 1988.
[19] P. Pengvanich *et al.*, "Effects of frequency chirp on magnetron injection locking," *Phys. Plasmas*, vol. 15, no. 7, Jul. 2008, Art. no. 073110.

Xiaojie Chen received the B.S. degree in information counter technology from the Southwest University of Science and Technology, Mianyang, China, in 2014, and the M.S. degree in radio physics from Sichuan University, Chengdu, China, in 2018, where he is currently pursuing the Ph.D. degree in communication systems and engineering.

His current research interests include injection-locking technology, high-power microwave combining, and multipactor suppression techniques.

Ze Yu received the B.S. degree in electronic science and technology from the North China University of Water Resources and Electric Power, Zhengzhou, China, in 2017. He is currently pursuing the M.S. degree in radio physics from Sichuan University, Chengdu, China.

His current research interest includes microwave engineering.

Hang Lin received the B.S. degree in electronic information engineering from Sichuan University, Chengdu, China, in 2016, where he is currently pursuing the Ph.D. degree in radio physics.

His current research interests include microwave circuits and microwave wireless power transmission.

Xiang Zhao received the B.S. degree in mathematics, the M.S. degree in radio physics, and the Ph.D. degree in biomedical engineering from Sichuan University, Chengdu, China, in 1994, 1997, and 2005, respectively.

In 1997, she joined the Department of Electronics Engineering, Sichuan University, where she has been a Professor with the College of Electronics and Information Engineering since 2012. She has authored or coauthored over 90 articles in the peer-reviewed journals and conferences and led a number of grant projects. Her research interests include statistical electromagnetics, electromagnetic compatibility modeling, and electromagnetic environment effects evaluation.

Changjun Liu (M'07–SM'09) received the B.S. degree in applied physics from Hebei University, Baoding, China, in 1994, and the M.S. degree in radio physics and the Ph.D. degree in biomedical engineering from Sichuan University, Chengdu, China, in 1997 and 2000, respectively.

From 2000 to 2001, he was a Post-Doctoral Researcher with Seoul National University, Seoul, South Korea. From 2006 to 2007, he was a Visiting Scholar with Ulm University, Ulm, Germany. Since 1997, he has been with the Department of Radio-Electronics, Sichuan University, where he has been a Professor since 2004. He has authored or coauthored one book, one chapter in a book, and more than 100 articles. He holds more than ten patents. His current research interests include microwave power combining of large-power vacuum components, microwave wireless power transmission, and microwave power industrial applications.

Dr. Liu was a recipient of several honors such as the outstanding Reviewer for the IEEE TRANSACTIONS ON MICROWAVE THEORY AND TECHNIQUES from 2006 to 2010, support from the Ministry of Education (MOE) under the Program for New Century Excellent Talents in University, China, from 2012 to 2014, the Sichuan Province Outstanding Youth Fund from 2009 to 2012, and named by Sichuan Province as an Expert with Outstanding Contribution. He serves on the Editorial Board for the *Chinese Journal of Applied Science*.